Charge transport in Weyl 2D materials

Halina Grushevskaya, George Krylov*

Faculty of Physics, Belarusian State University, 4 Nezaleznasti ave., Minsk, 220030, Belarus

*Corresponding author

DOI: 10.5185/amp.2018/980
www.vbripress.com/amp

Abstract

Earlier proposed theoretical approach to the band theory of two-dimensional (2D) semimetals based on a self-consistent Dirac–Hartree–Fock field approximation, a quasi-relativistic model of Dirac 2D material in the tight-binding approximation with accounting of π-electron orbitals has been developed. Fermi velocity becomes an operator within this approach. The model admits a Weyl type of charge carriers described by chiral bispinors. Since Weyl fermions in a pair have equal in absolute but opposite in sign values of pseudo- helicity (topological charge), due to the topological charge conservation law Weyl fermions can decay only in pairs. Therefore, in contrast to the Dirac electrons and holes, Weyl fermions turns out to be long-lived quasiparticles. Stability of the band structure of the 2D materials is stipulated by coupling of valley currents with pseudospins of chiral Weyl charge carriers. Numerical simulation of the band structure has been performed for the atomically thin model layers (monolayers) of C and Pb atoms, taking into account only corrections up to 4th order in wave vector. Such features of the band structure of 2D semimetals as appearance of three pairs of Weyl-like nodes; partial removal of Dirac cone and replicas degeneration are shown to be naturally explained within the developed formalism. Since the Dirac cone replica is split into oppositely directed cones, the monolayers of atoms C and Pb are 2D materials, in which pairs of Weyl massless fermions can be excited. Simulation of charge transport in these materials has been performed.

Keywords: 2D semimetal, dirac–hartree–fock self-consistent field approximation, weyl-like nodes, fermi velocity operator appropriate.

Introduction

Exotic properties of the so called Dirac fermion materials such as graphene [**1,2**] and some others [**3-10**] are of theoretical interest after years of their discovery. The reasons, among pure theoretical interest to analogs of known relativistic quantum field theory (QFT) objects in solid state physics, were their promising suitability for the purposes of quantum information processing [**11,12**] and potential applications in spintronics [**13,14**] and nanoelectronics (see, e.g. [**15,16**] and references therein). This occurs primarily due to the existence of non-trivial topological characteristics in such systems and is stipulated typically by some effective dimensional reduction, such e.g., as geniune two-dimensionality of graphene [**17**], the existence of the Dirac points in the Brillouin zone of some 3D materials [**3-7,18**], dimensionality reduction via an effective magnetic field (see e.g., [**19**] and appropriate references therein). In its turn, it leads to regular search for even more sophisticated and non-existing in High Energy Physics objects like Majorana fermions [**20-22**], Weyl nodes [**23,24**], Fermi arcs [**25**] and so on [**26**]. There are some experimental evidence that low energy collective excitations with such features could really be observed in some electron strongly correlated systems [**27-31**].

Specifically to graphene, one of the still most intriguing aspect in its theoretical description is very good applicability of a very simple two dimensional massless Dirac fermion model (2D DFM) proposed yet by P.R. Wallace [**1**] and further developed by R.W. Semenoff in [**3**2]. It is based on the non-relativistic tight-binding approximation (TBA) and leads qualitatively and quantitatively to rather good correspondence of theoretical and experimental data in most experimental situations (see e.g., reviews [**17,33,34**] and references therein). The simulations performed with modern band structure *ab initio* software systems also confirm it applicability at least for several lower bands [**35**]. At the same time it is well known that attempts to use non-relativistic codes for band structure simulations lead to serious divergence of calculated and observable material properties [**36**]. It is the point why all modern software in the field like AbInit, FPLO, WIEN2k, VASP uses some variants of the Dirac equation or related ones solvers. With the goal to match these two statements, in [37-43] it has been proposed an approach to graphene band structure simulation which is based on quasi-relativistic Dirac–Hartree–Fock self-consistent field, accounting of π-electron orbitals in TBA with an additional assumption on anti-ferromagnetic pseudo-spin ordering of graphene sublattices. The main goal achieved is that the consequent

relativistic quantum field theory description with account of the exchange interactions and appropriately developed TBA leads to equations which are very similar to that of 2D DFM except that the Fermi velocity is dependent on the exchange interactions and turns out to be an operator rather than a scalar one [37-38]. In this way it is possible to explain small charge carrier mass asymmetry [38], to demonstrate partial Dirac band symmetry break in graphene [40,41,43], and the existence of Weyl-like nodes in the graphene model with power series expansion approximation for the exchange operator [38], and to manifest the possibility of the eight-fold splitting of the Dirac cone on sub-replicas [42]. Sufficient generality of the proposed approach [38-43] allows to apply it for the consistent description of non-equilibrium properties of these materials. This will be the primary goal of the paper with special attention to the single layer graphene case.

Fundamentals

We begin by brief outlining the semimetal monolayer model with partial unfolding of the Dirac bands [38-41]. Hereafter, graphene will be used as a typical representative; other will be mentioned especially if necessary. Graphene honeycomb lattice consisting of two interpenetrating triangle lattices is shown schematically in **Fig. 1.** (Atoms in the sub-lattices are marked with *A*, *B* indexes and associated with them direction of a "pseudo-spin").

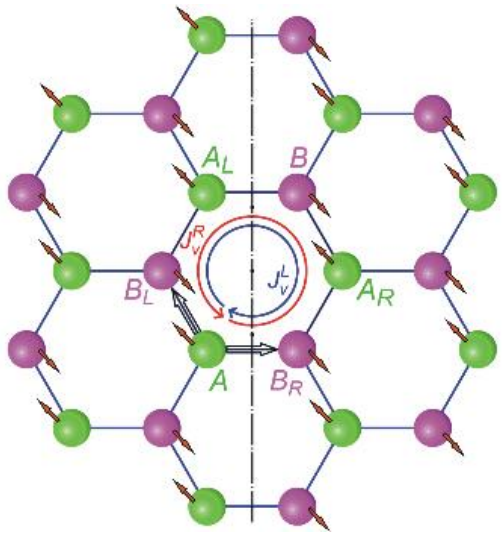

Fig. 1. Graphene honeycomb lattice, comprised of two sub-lattices {*A*} with spin "up" and {*B*} with spin "down". Right and left valley currents J_v^R and J_v^L are shown as circular curves with arrows. Double arrows from site *A* to site B_L and from *A* to B_R indicate clockwise and anti-clockwise directions. The axis of mirror reflection from A_R to B_L is marked by dash-dotted line. (in color)

The existence of Dirac cones in the Dirac points *K*, *K'* of the Brillouin zone is known to be a prominent feature of the graphene band structure and this corresponds to massless collective excitations in the model [17]. We designate these point as K_A,K_B in what follows.

The pseudo-helicity conservation law forbids massless charged carriers to be in lattice sites with the opposite signs of pseudo-spin making possible the existence of valley currents due to jumps through the forbidden sites. Pseudo-spin and valley current coupling can be determined as follows [42]. A particle can travel from a lattice site *A* to, for example, a lattice site A_R through right or left sites B_R or B_L, respectively.

Particle description in the right and left reference frames should be the same. As a result, bispinor wave function Ψ' should to be chosen in Majorana representation, and its upper and lower spin components ψ', $\dot{\psi}'$ should be transformed by the left and right representations of the Lorentz group as:

$$\Psi' = \begin{pmatrix} \psi'_{\sigma} \\ \dot{\psi}'_{-\sigma} \end{pmatrix} = \begin{pmatrix} e^{\frac{\kappa}{2}\vec{\sigma}\cdot\vec{n}}\psi_{\sigma} \\ e^{\frac{\kappa}{2}(-\vec{\sigma})\cdot\vec{n}}\dot{\psi}_{-\sigma} \end{pmatrix} \quad (1)$$

The wave-function $\P^{\dagger}_{\sigma}(\vec{r}_A)|0,+\sigma\rangle$ of a particle located on the site *A*, behaves as a component ψ_{σ}, while the wave-function $\dot{\chi}^{\dagger}_{-\sigma}(\vec{r}_B)|0,-\sigma\rangle$ of a particle located on the site *B* behaves as a component $\dot{\psi}_{-\sigma}$ of the bispinor (1).

Let us designate the two-dimensional spin of quasi-particles in valleys K_A and K_B as $\vec{S}_{AB} = \hbar\vec{\sigma}_{AB}/2$ and $\vec{S}_{BA} = \hbar\vec{\sigma}_{BA}/2$, respectively, where the vector of transformed Pauli matrices will be defined later. A valley current J_v^R, on the right or left closed contour in figure 1 $\{A \to B_R \to A_R \to B \to A_L \to B_L \to A\}$ is created by an electron (hole) with pseudo-angular momentum $\vec{l}_{AB_R}$ and momentum $\vec{p}_{AB_R}$. Pseudo-helicity of bispinors (1), describing the particles right or left the from lattice site *A*, can be defined by the expressions, which are analogous to ordinary relativistic ones in QFT as [46]:

$$h_{B_R A} \equiv \vec{p}_{AB_R} \cdot \vec{S}_{B_R A} \quad (2)$$

and similar for the left contour.

Let *P* be a parity operator, which mirrors the bispinor (1) with respect to the line passing through the points *A* and *B*. The pseudo-helicity of the mirrored bispinor is defined as

$$Ph_{B_R A_R}P = h_{A_L B_L} = \vec{p}_{B_L A_L} \cdot \vec{S}_{A_L B_L}. \quad (3)$$

Pseudo-helicity h_{AB} does not change its value while the valley momentum and the pseudo-spin change signs: $\vec{p}_{A_L B_L} = -\vec{p}_{B_R A_R}$ and $\vec{S}_{A_L B_L} = -\vec{S}_{B_R A_R}$, so it can be expressed through the projection $\tilde{M}_{AB} = \vec{\sigma}_{BA} \cdot (\vec{l}_{AB} + \hbar\vec{\sigma}_{BA}/2)$ of the total angular momentum on the direction of the spin $\vec{\sigma}_{BA}$ as [47,51]:

$$\vec{\sigma}_{BA}\cdot\vec{p}_{AB}=\sigma^{r}_{BA}\left(p_{r,BA}+\div\frac{\tilde{M}_{AB}}{r}-\hbar/2\right)$$
$$=\sigma^{r}_{BA}\left(p_{r,BA}+\div\frac{\vec{\sigma}_{BA}\cdot\vec{l}_{AB}}{r}\right), \quad (4)$$

where σ^{r}_{BA} and $p_{r,BA}$ are radial components of the spin and the momentum, respectively. In accord with the last relation, the pseudo-spin-orbit scalar $\vec{\sigma}_{BA}\cdot\vec{l}_{AB}$ describes the coupling of the spin with the valley currents flowing along a closed loop in clockwise or anticlockwise directions, as is shown in figure 1. As a result, there exists a preferred direction along which the "spin projection" of the bispinor (1) is not changed after transition from one moving reference frame into another. At this, the spin of a particle precesses and this transformation of the electron and hole into each other in an exciton is a pseudo-precession. In the model, the orientation of non-equilibrium spin of the states of monolayer graphene in electromagnetic fields may be retained for a long time due to prohibition of change for exciton pseudo-helicity. Pseudo-precession is possible, if spins of p_z-electrons are anti-ordered (pseudo-antiferromagnetic ordering). Therefore, the pseudo-spin precession of the exciton can be implemented through the exchange interaction. Starting from a representation of the secondary quantization and the Dirac–Hartree–Fock self-consistent field approximation, it is possible to derive [38,39] the following eigenproblem for graphene secondary quantized wave function $\hat{\chi}^{\dagger}_{-\sigma_A}$ in quasi-relativistic approximation in leading c^{-1} order term series expansion

$$\left\{\vec{\sigma}\cdot\vec{p}\,\hat{v}_F^{qu}-\frac{1}{c}\left(i\Sigma^{x}_{rel}\right)_{AB}\left(i\Sigma^{x}_{rel}\right)_{BA}\right\}\hat{\chi}^{\dagger}_{-\sigma_A}(\vec{r})|0,-\sigma\rangle$$
$$=E_{qu}(\vec{p})\hat{\chi}^{\dagger}_{-\sigma_A}(\vec{r})|0,-\sigma\rangle, \quad (5)$$

where c is the speed of light, the Fermi velocity operator $\hat{v}_F^{qu}$ is defined as

$$\hat{v}_F^{qu}=\left[\left(\Sigma^{x}_{rel}\right)_{BA}+c\hbar\vec{\sigma}\cdot(\vec{K}_A+\vec{K}_B)\right], \quad (6)$$

$\left(\Sigma^{x}_{rel}\right)_{BA},\left(\Sigma^{x}_{rel}\right)_{AB}$ are relativistic exchange operators defined as [38-40]

$$\left(\Sigma^{x}_{rel}\right)_{AB}\hat{\chi}^{\dagger}_{\sigma_B}(\vec{r})|0,\sigma\rangle=\sum_{i=1}^{N_v N}\int d\vec{r}_i\hat{\chi}^{\dagger}_{\sigma_i B}(\vec{r})|0,\sigma\rangle$$
$$\times<0,-\sigma_i|\hat{\chi}^{\dagger}_{-\sigma_i^A}(\vec{r}_i)V(\vec{r}_i-\vec{r})\hat{\chi}_{-\sigma_B}(\vec{r}_i)|0,-\sigma_{i'}>, \quad (7)$$

$V(\vec{r}_i-\vec{r})$ is the Coulomb interaction between two valence electrons with radius-vectors $\vec{r}_i$ and $\vec{r}$; N is a total number of atoms in the system, N_v is a number of valence electrons in an atom. Eq. (5) can be transformed to more convenient form after performing non-unitary transformation of the wave function

$$\hat{\tilde{\chi}}^{\dagger}_{-\sigma_A}|0,-\sigma\rangle=\left(\Sigma^{x}_{rel}\right)_{BA}\hat{\chi}^{\dagger}_{-\sigma_A}|0,-\sigma\rangle. \quad (8)$$

Then we get

$$\left\{\vec{\sigma}^{AB}_{2D}\cdot\vec{p}_{BA}-c^{-1}\widehat{\widetilde{\Sigma}}_{BA}\Sigma_{AB}\right\}\hat{\tilde{\chi}}^{\dagger}_{-\sigma_A}(\vec{r})|0,-\sigma\rangle$$
$$=E_{qu}(p)\hat{\tilde{\chi}}^{\dagger}_{-\sigma_A}(\vec{r})|0,-\sigma\rangle\ , \quad (9)$$

where 2D vector $\vec{\sigma}^{AB}_{2D}$ of the transformed Pauli matrices reads $\vec{\sigma}^{AB}_{2D}=\left(\Sigma^{x}_{rel}\right)_{BA}\vec{\sigma}\left(\Sigma^{x}_{rel}\right)^{-1}_{BA}$, $\vec{p}_{BA}\hat{\tilde{\chi}}^{\dagger}_{-\sigma_A}=\left(\Sigma^{x}_{rel}\right)_{BA}\vec{p}\left(\Sigma^{x}_{rel}\right)^{-1}_{BA}\hat{\tilde{\chi}}^{\dagger}_{-\sigma_A}$, $\tilde{E}_{qu}=E_{qu}/\hat{v}_F^{BA}$, $\hat{v}_F^{BA}=\left(\Sigma^{x}_{rel}\right)_{BA}$, $\widehat{\widetilde{\Sigma}}_{BA}\Sigma_{AB}\equiv\left(\Sigma^{x}_{rel}\right)_{BA}\left(i\Sigma^{x}_{rel}\right)_{AB}\left(i\Sigma^{x}_{rel}\right)_{BA}\left(\Sigma^{x}_{rel}\right)^{-1}_{BA}=\left(i\Sigma^{x}_{rel}\right)_{BA}\left(i\Sigma^{x}_{rel}\right)_{AB}$.

Formally, one can see that eq. (9) is very similar to that of 2D DFM except of changed meaning of Pauli matrices, momentum operator as well as a small (of order c^{-1}) anisotropic mass term as a last summand in left hand side of eq. (9). The equation (9) allows to fulfilled the simulations of the band structure in the model. The simulations have been performed in the nearest neighbor TBA [38,43]. This approximation correctly predicts the graphene band structure in the energy range of about ±1 eV [52]. This turns out to be sufficient for our purposes. The expressions for the exchange between $\pi(p_z)$-electrons only have been used, then the exchange terms have been expanded into a power series on wave vectors near Dirac point up to the four power in $\vec{q}$, where $\vec{q}=\vec{p}/\hbar-\vec{K}_{A(B)}$. The simulation results for graphene and Pb model monolayer are shown in **Fig. 2.** As one can see, splitting of the Dirac cone on replicas takes place and Weyl like-nodes appear, visible singularities are originated from non-invertibility of the $\left(\Sigma^{x}_{rel}\right)_{BA},\left(\Sigma^{x}_{rel}\right)_{AB}$ matrixes for some wave vectors in $\vec{q}$-space. For graphene, the Weyl-like nodes seems to be far enough from the Dirac cone apex, as a result their appearance can be considered as only qualitative statement because of restricted applicability of the TBA in this region, while for Pb monolayer they are much closer to Dirac point and appropriate effects could be experimentally observable.

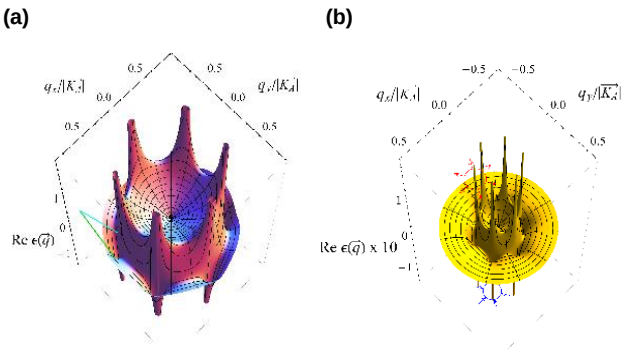

Fig. 2. Splitting of the Dirac cone: for graphene (a) and Pb monolayer (b). One of the six pairs of Weyl-like nodes for electron and holes Dirac cones; source and sink are indicated.(in color)

The action of the exchange operator on a vector in $\vec{q}$ -space is the stretch and rotation, the action is different for electron and holes that results in almost $\pi/2$ rotation of electrons and holes bands in respect to each others [40-42]. Now, we look at the action of the exchange operator applied to sum of electron and hole Dirac bands. Accounting of the fact that $\vec{\sigma}_{AB}\cdot\vec{p}_{BA}$ is a helicity operator, the action of $\left(\Sigma^{x}_{rel}\right)_{BA}$ can be considered as non-equilibrium transfer of a carrier into a state of same pseudo-spirality, and doubled action as non-equilibrium forth and back jump. As one can see from inset in the **Fig. 3,** the Dirac point becomes hyperbolic one due to carriers asymmetry and therefore unstable after single exchange operator action on the Hamiltonian.

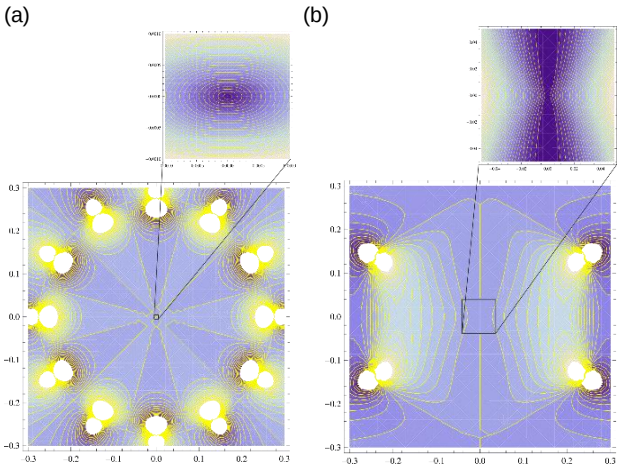

Fig. 3. Action of the exchange operators on a sum of electron and holes Dirac bands demonstrating the stability loss of the Dirac point. (a) original sum of the bands, (b) result of the one exchange operator action on the Hamiltonian. (in color).

Based on the model proposed and the simulation results on the band structure, it is possible to develop methods for calculation of the conductivity of the material that will be the goal of the following section.

Methods

Conductivity can be considered as a coefficient linking the current density with the applied electric field in linear regime of response. To reach the goal, several steps should be performed. First, it one has to subject the system by an electromagnetic field, this can be implemented by standard change to canonical momentum $\vec{p}\mapsto\vec{p}-e\vec{A}$ in eq. (5) where $\vec{A}$ is the vector-potential of the field.

The expression for current operator can be written in accord with known quasi-relativistic expression for current in quantum mechanics [53]

$$j_i^{pseudo}(x)=e\psi^{\dagger}(x')v^{i}_{x'x}\psi(x)$$
$$-\frac{e^2}{c}\psi^{\dagger}(x')\left(m^{ij}\right)^{-1}\psi(x)A_j,\quad x'\to x, \tag{10}$$

where $\vec{v}=v_i, i=1,2$ is the velocity operator determined by a derivative of the Hamiltonian $\hat{H}(\vec{p})$ over the momentum operator: $\vec{v}=\partial\hat{H}(\vec{p})/\partial\vec{p}$, $\psi(x)$ is the secondary quantized fermion field. In the interaction representation a potential V of the coupling between electromagnetic field $\vec{A}$ and current $\psi^{\dagger}(x')v^{i}_{x'x}\psi(x)$ is given by

$$V=-\frac{e}{c}\int\psi^{\dagger}(x')v^{i}_{x'x}\psi(x)A_i(x)dt\,d\vec{x}. \tag{11}$$

After tedious but simple algebra one can find the following expression for the current in our model:

$$c\,j_i=e\chi^{\dagger}_{+\sigma_B}(x^{+})v^{i}_{x^{+}x^{-}}\chi_{+\sigma_B}(x^{-})$$
$$-\frac{e^2A_i}{c\,\Sigma_{AB}\Sigma_{BA}(\vec{p}_{AB}-e\vec{A}/c)}\chi^{\dagger}_{+\sigma_B}(x^{+})\chi_{+\sigma_B}(x^{-})$$
$$+\frac{e\hbar}{2\tilde{\Sigma}_{AB}\Sigma_{BA}(\vec{p}_{AB}-e\vec{A}/c)}\left|\vec{\nabla}\times\chi^{\dagger}_{+\sigma_B}(x^{+})\vec{\sigma}\chi_{+\sigma_B}(x^{-})\right|_i, \tag{12}$$

where the following notions are introduced $\tilde{\Sigma}_{AB}\Sigma_{BA}=-\left(\Sigma^{x}_{rel}\right)_{BA}\Sigma_{AB}\Sigma_{BA}\left(\Sigma^{x}_{rel}\right)^{-1}_{BA}=-\Sigma_{BA}\Sigma_{AB}$, $x^{\pm}=x\pm\grave{o}, x=\{\vec{r},t_0\}, t_0=0, \grave{o}\to 0$. Transforming the last term in (12) we get the three components for the current, namely ohmic, Zitterbewegnung and spin-orbit ones (up to a common factor c^{-1}) as

$$c\,j_i^{Ohm}=e\chi^{\dagger}_{+\sigma_B}(x^{+})v^{i}_{x^{+}x^{-}}\chi_{+\sigma_B}(x^{-}), \tag{13}$$

$$c\,j_i^{ZB}=-\frac{e^2A_i}{c\tilde{\Sigma}_{AB}\Sigma_{BA}(\vec{p}_{AB}-e\vec{A}/c)}\chi^{\dagger}_{+\sigma_B}(x^{+})\chi_{+\sigma_B}(x^{-}) \tag{14}$$

$$c\,j^{spin-orbit}_{2(1)}=(-1)^{1(2)}\frac{ie}{2}v^{1(2)}_{x^{+}x^{-}}\chi^{\dagger}_{+\sigma_B}(x^{+})\sigma_z\chi_{+\sigma_B}(x^{-}). \tag{15}$$

These components correspond to Ohm law, and contributions from polarization and magneto-electric effects, respectively.

To perform quantum-statistical averaging for the case of non-zero temperature, one can use an approach developed in [45,50] when it has been used for the 2D DFM model. There was an only ohmic term to be accounted in [45,50], the Hamiltonian was also much simpler as well. For our model the Fourier-Laplace component of ohmic conductivity is expressed as

$$\sigma_{ij}(\omega,k)=\frac{ie^2}{\pi^2}\left\{\sum_{a=1,2}\int\frac{v^{i}_{aa,AB(BA)}v^{j}_{aa,AB(BA)}}{\left[\varepsilon_a(\vec{p}_{+})-\varepsilon_a(\vec{p}_{-})\right]}\right.$$
$$\left.\times\frac{f\left[\varepsilon_a(\vec{p}_{-})\right]-f\left[\varepsilon_a(\vec{p}_{+})\right]}{\left[\omega-\varepsilon_a(\vec{p}_{+})+\varepsilon_a(\vec{p}_{-})\right]}d^2\vec{p}+2\omega\right. \tag{16}$$

$$\times\int \frac{v^{i}_{12,AB(BA)}v^{j}_{21,AB(BA)}\left\{f\left[\varepsilon_1(\vec{p}_-)\right]-f\left[\varepsilon_2(\vec{p}_+)\right]\right\}}{\left[\varepsilon_2(\vec{p}_+)-\varepsilon_1(\vec{p}_-)\right]\left[\omega^2-\left(\varepsilon_2(\vec{p}_+)-\varepsilon_1(\vec{p}_-)\right)^2\right]}d^2\vec{p}\Bigg\}.$$

Here $\varepsilon_a(p_\pm)=\Re e\, E_{qu}(p_\pm)_a$, $a=1,2$ are conduction and valence electrons eigenenergies in the appropriate model; $f(\varepsilon_a)$, $a=1,2$ is a quasi-particle Fermi-Dirac distribution function; a-th bands are the valence $(a=1)$ and conduction $(a=2)$ bands, $i(j)=x,y$, $\vec{v}_{AB(BA)}=v_F\dfrac{\partial\left[\vec{\sigma}^{BA(AB)}_{2D}\cdot\vec{p}_{AB(BA)}\right]}{\partial\vec{p}}$, v_F is the Fermi velocity, $\vec{p}_\pm=\vec{p}\pm\vec{k}/2$.

In the following section we represent simulation results on ohmic contribution to conductivity and compare results of [45,50] and those of our model.

Results and discussion

Simulations of the conductivity have been performed for two variant of approximation to the exchange operator. The first one already mentioned above is the series expansion of the exchange matrices on deviation of wave vector from the Dirac point up to 4th order in $\vec{q}$. As it has been shown in [38-41] this approximation leads to a small imaginary part for the energy (spectral line width), this in fact not very bad as it effectively corresponds to a finite decay. Moreover such small imaginary part corrections should be added when calculating with the use of eq. (16) in order to shift the integration line (p-axis) aside the poles of integrand. For the simulations we use the spectral line width equals to 1 K. The second approximation is the use of the exchange interaction matrices calculated based on π_z-orbital wave functions with full exponents and with non-zero phases (see the detail of the approximation in [40-43]). The last approximation holds real eigenenergies for all wave vectors.

The frequency dependencies of the real and imaginary part of optical conductivity ($|\vec{k}|=0$) for temperatures $T=3K$ and $T=200K$ are shown in **Fig. 4.**

Chemical potential μ has been chosen as μ=135K for $T=3K$ case and μ=33K for $T=200K$. Red dashed line corresponds to calculations based on the conductivity formula in [45,50] , green line is the first approximation for our model, blue line is the second approximation for $T=3K$. Dashed-black line corresponds to first approximation and $T=200K$ and demonstrates that the fast fall down of the first approximation scheme is due to non-zero imaginary part contribution to the energy accompanied with a finite line width chosen. Comparing results for frequency dependencies of our model and the paper [45,50] one can conclude the good coincidence of both models in the optical frequency range.

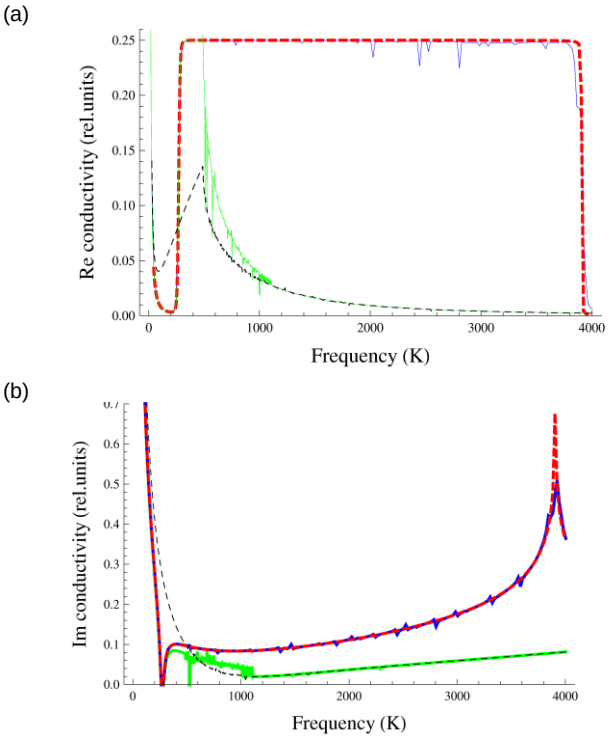

Fig. 4. Frequency dependencies of the real (a) and imaginary (b) part of the conductivity for the model [45,50] at T=3K (red line) and for our model (green and black dashed lines for the first approximation at T=3K and T=200K respectively, and blue line for the second approximation at T=3K), see detail in text.(in color)

For attacking the so called "minimal conductivity" problem [48, 49] it is important to obtain the dependence of the conductivity for very small frequency and non-vanishing wave vectors. Such a comparison for the two models for $T=100K, \mu=1K$ is demonstrated in **Fig. 5** for the frequency $\hbar\omega=10^{-10}K$.

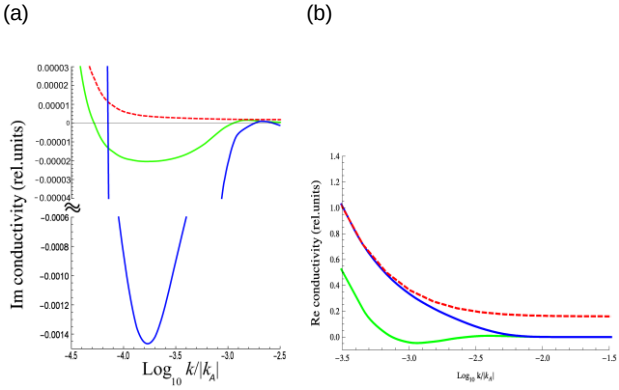

Fig. 5. Imaginary (a) and real (b) parts of longitudinal conductivity vs Logarithm of the wave number k normalized on $|k_A|$ in two approximations of our model (solid blue curves) and model of [45,50] (dashed red curves). The chemical potential equals to 1 K at temperature 100K and frequency $\hbar\omega=10^{-10}K$.(in color)

In the model [45,50] the spatial dispersion of the dielectric permeability $\varepsilon(\omega,k)$ (imaginary part of conductivity) of non-doped graphene is positive. 2D

According simulations performed based on density functional theory [54] and a single-pole approximation for small momenta used in [55], the Dirac fermion model overestimates the dielectric polarization but screening remains dielectric one. Therefore the plasmon mode for which $\varepsilon(\omega,k)\le 0$ and hence electronic screening are absent. Contrary to that in our model with spatial dispersion, there exist plasmon modes at low frequencies $\omega\to 0$ as the dielectric permeability $\varepsilon(\omega,k)$ can gain zero and negative values, green (the first approximation) and blue (the second one) lines in figure 5a. Hence, the pure graphene is able to screen in electrophysical range.

To obtain dc-conductivity σ^{dc} of graphene (also called as minimal conductivity) one has to performed inverse Fourier transform for spatial component $\sigma(\omega=0,\vec{k})$. As one can see from figure 5b, the model [45,50] gives asymptotically a positive constant for the conductivity for high wave numbers resulting in zero value for dc-conductivity. For our model the *k*-dependence of real part of conductivity demonstrates fast decrease to zero that provides a finite non-zero value for the minimal conductivity.

Conclusion

Summarizing our finding, the earlier developed quasi-relativistic approach to graphene band structure simulation has been successfully applied to describe peculiarities in band structure and features of charge transport forp Weyl semimetal model systems. On an example of graphene it has been demonstrate that the developed model can be useful to explain the existence of plasmonic modes in pure graphene as well as to be a starting point to understand the existence of minimal conductivity of graphene.

Acknowledgements

This work was supported in part by the State Program for Fundamental Research of Belarus "Convergence-2020".

Author's contributions

Both authors equally contribute to the paper content. Authors have no competing financial interests.

References

1. Wallace, P. R.; Phys. Rev. 1947, 71, 622 **DOI:** 10.1103/PhysRev.71.622
2. Novoselov, K. S.; Geim, A. K.; Morozov, S. V.; Jiang, D.; Zhang, Y.; Dubonos, S. V.; Gregorieva, I. V.; Firsov, A. A.;, Science 2004, 306, 666.
3. Cohen, M. H.; Blount, E. I.; *Philos. Magazine* **1960**, *5*, 115. **DOI**: 10.1080/14786436008243294
4. Lenoir, B.; Cassart, MMichenaud, .; J.-P.; Scherrer, H.; Scherrer, S.*; J. of Phys. and Chem. Solids* **1996**, *57*, 89. **DOI**: 10.1016/0022-3697(95)00148-4
5. Wang, Z.; Sun, Y.; Chen, X.; Franchini, C.; Xu, G.; Weng, H.; Dai, X.; Fang, Z.; *Phys. Rev*. **2012**, *B85*, 195320. **DOI**: 10.1103/PhysRevB.85.195320.
6. Liu, Z. K.; Zhou, B.; Wang, Z. J.; Weng, H. M.; Prabhakaran, D.; Mo, S. K.; Zhang, Y.; Shen, Z. X.; Fang, Z.; Dai, X.; Hussain, Z.; Chen, Y. L.; *Science* **2014**, *343*, 864. **DOI**: 10.1126/science.1245085.
7. Wang, Z.; Weng, H.; Wu, Q.; Dai, X.; Fang, Z.; *Phys. Rev*. **2013**,B88, 125427. **DOI**: 10.1103/PhysRevB.88.125427.
8. Teo, J. C. Y.; Fu, L.; Kane, C. L.; *Phys. Rev*. **2008**, *B78*, 045426. **DOI**: 10.1103/PhysRevB.78.045426.
9. Xu, S.-Y.; Xia, Y.; Wray, L.A.; Jia, S.; Meier, F.; Dil, J. H.; Osterwalder, J.; Slomski, B.; Bansil, A.; Lin, H.; Cava, R. J.; Hasan, M. Z.; *Science* **2011**, *332*, 560 **DOI**: 10.1126/science.1201607
10. Sato, T.; Segawa, K.; Kosaka, K. ; Souma, S.; Nakayama, K.; Eto, K.; Minami, T.; Ando, Y.; Takahashi, T.; Nature Phys. 2011, 7, 840 **DOI**: 10.1038/nphys2058
11. Paudel, H. P.;. Leuenberger, M. N.; Phys. Rev. 2013, B 88, 085316 **DOI**: 10.1103/PhysRevB.88.085316
12. Zhi-Rong Lin, Guo-Ping Guo, Tao Tu, Qiong Ma and Guang-Can Guo ; Quantum Computation with Graphene Nanostructure, in Physics and Applications of Graphene - Theory, Dr. Sergey Mikhailov (Ed.), InTech, 2011 **DOI:** 10.5772/15097
13. Han, W.; Kawakami, R. K.; Gmitra, M.; Fabian, J.; *Nature Nanotech*. **2014**, *9*, 794 **DOI**: 10.1038/nnano.2014.214
14. Pesin, D.; MacDonald, A. H.; *Nature. Mat.* **2012**, *11*, 409 **DOI**: 10.1038/nmat3305
15. Schwierz, F. *Nature Nanotech*. **2010**, *5*, 487 **DOI:** 10.1038/nnano.2010.89
16. Xiao-Liang Qi and Shou-Cheng Zhang, *Rev. Mod. Phys*. **2011**, *83*, 1057 **DOI:**10.1103/RevModPhys.83.1057
17. Neto, A. H. C.; Guinea, F.; Peres, N. M. R.; Novoselov, K. S.; Geim, A. K.; *Rev. Mod. Phys*. **2009**, *81*, 109. **DOI**: 10.1103/RevModPhys.81.109.
18. Edel'man, V. S.; *Sov. Phys. Uspekhi* **1977**, *20*, 819. **DOI**: 10.1070/PU1977v020n10ABEH005467
19. Miranski V.A., Shovkovy I.A.; *Phys. Rept* **2015**, *576*, 1 **DOI:** 10.1016/j.physrep.2015.02.003
20. Majorana, E.; *Nuovo Cimento* **1932,** *9*, 335
21. Dóra, B.; Gulácsi, M.; Sodano, P.; *Phys. Status Solidi* **2009**, *RRL 3*, 169 **DOI**: 10.1002/pssr.200903161
22. San-Jose, P.; Lado, J. L.; Aguado, R.; Guinea, F.; Fernández-Rossier, J.; *Phys. Rev*. **2015,** *X5*, 041042 **DOI**: 10.1103/PhysRevX.5.041042
23. Wilczek, F.; *Phys. Today* **1998**, *51*, 11
24. Balents, L.; *Physics* **2011**, *4*, 36. **DOI**: 10.1103/Physics.4.36
25. Wan, X.; Turner, A. M.; Vishwanath, A.; Savrasov, S. Y.; *Phys.Rev*. **2011**, *B 83*, 205101. **DOI**: 10.1103/PhysRevB.83.205101
26. Bradlyn, B.; Cano, J.; Wang, Z.; Vergniory, M. G. ; Felser, C.; Cava, R. J.; Bernevig, B. A. *Science* **2016**, *353*, 6299 **DOI:** 10.1126/science.aaf5037
27. Xu, S.-Y.; Belopolski,I; Alidoust,N.; Neupane,M.; Bian, G.; Zhang,C.; Sankar, R.; Chang, G.; Yuan, Z.; Lee, C.-C.; Huang, Sh.-M.; Zheng,H; Ma, J.; Sanchez, D. S.; Wang,BK. Bansil,A.; Chou,F.; Shibayev, P.P.; Lin, H.; Jia, S.; Hasan M. Z.; *Science* **2015**, *349*, 613 **DOI:** 10.1126/science.aaa9297
28. Lv, B.Q.; Xu, N.; Weng, H. M.; Ma, J. Z. ; Richard, P.; Huang, X. CZhao, .; L. X. ; Chen, G. F.; Matt, C. E. ; Bisti, F.; Strocov, V. N.; Mesot, J.; Fang, Z. ; Dai, X. Qian, ;T.; Sh, M.; Ding, H.; *Nature Physics* **2015**, *11*, 724 **DOI:** 10.1038/NPHYS3426
29. Nadj-Perge, S.; Drozdov, I.K.; Li, J; Chen, H.; Jeon, S.; Seo, J.; MacDonald, A.H.; Bernevig B.A.; Yazdani, A.; *Science* **2014** *346*, 602 **DOI:** 10.1126/science.1259327
30. Lu, L; Wang, Z; Ye, D; Ran, L; Fu, L; Joannopoulos, J.D; Soljačić, M; *Science* **2015**, *349*, 622 **DOI:** 10.1126/science.aaa9273
31. Yang, S. A.; SPIN 2016, 1640003 **DOI:** 10.1142/S2010324716400038
32. Semenoff, G.W. *Phys. Rev. Lett*. **1984,** *53*, 2449 **DOI:** 10.1103/PhysRevLett.53.2449

33. Peres, N M R; *J. Phys.: Condens. Matter* **2009**, *21*, 323201 **DOI:** 10.1088/0953-8984/21/32/323201
34. Andrei, E.Y.; Li, G.; Du, X. *Rep. Prog. Phys* **2012**, *75*, 056501 **DOI:** 10.1088/0034-4885/75/5/056501
35. Kogan, E. ; Nazarov, V. U.; Silkin, V. M.; Kaveh, M.; *Phys. Rev*. **2014**, *B 89*, 165430 **DOI**: 10.1103/PhysRevB.89.165430
36. Eschrig, H.; Richter, M.; Opahle, I. Theor. and Comput. Chem. **2004,** *13*, 723 **DOI:** 10.1016/S1380-7323(04)80039-6
37. Grushevskaya, H.V.; Krylov, G.G.; *J. Nonlinear Phenom. Complex Syst*. **2013**, *16*, 189
38. Grushevskaya, H.V.; Krylov, G. *J. Mod. Phys.* **2014**, *5*, 984 **DOI:** 10.4236/jmp.2014.510100
39. Grushevskaya, H.V.; Krylov, G.G.; Graphene: Beyond the Massless Dirac's Fermion Approach, in: Nanotechnology in the Security Systems, NATO Science for Peace and Security Series C: Environmental Security, Bonća J.; Kruchinin, S. (eds.), Springer Science+Business Media, Dordrecht, Chapter 3, **2015**. P. 21-31. **DOI:** 10.1007/978-94-017-9005-5_3
40. Grushevskaya, H.V.; Krylov, G,*; J. Nonlinear Phenom. Complex Syst.* **2015**, *18*, 266
41. Grushevskaya, H.V.; Krylov, G.; Gaisyonok, V.A.; Serow, D.V.; *J. Nonlinear Phenom. Complex Syst*. **2015,** *18*, 81
42. Grushevskaya, H.; Krylov, G; *Symmetry* **2016**, *8*, 60 **DOI:** 10.3390/sym8070060
43. Grushevskaya, H. V.; Krylov, G. G.; *Int. J. Mod. Phys.*, **2016,** *30*, 1642009 **DOI:** 10.1142/S0217979216420091
44. Grushevskaya, H. V.; Krylov, G . G .; Electronic Structure and Transport in Graphene: QuasiRelativistic Dirac-Hartree-Fock Self-Consistent Field Approximation In: Graphene Science Handbook: Electrical and Optical Properties. Vol. 3. Eds. M. Aliofkhazraei, N. Ali, W.I. Milne, C.S. Ozkan, S. Mitura, J.L. Gervasoni., Taylor and Francis Group, CRC Press, USA, UK, Chapter 9., **2016,** 117-132.
45. Falkovsky, L.A.; *Phys.-Uspekhi* **2008**, *51*, 887
46. Peskin, M.E.; Schroeder, D.V.; An Introduction to Quantum Field Theory; Addison-Wesley Publishing Company: Oxford, UK, **1995**.
47. Krylova, H. Hursky, L. Spin polarization in strong-correlated nanosystems. LAP LAMBERT Academic Publishing, Saarbru¨cken, **2013**.
48. Ziegler, K. *Phys. Rev*. **2007**, *B. 75*, 233407.
49. Ando, T.; Zheng, Y.; Suzuura, H.; *J. Phys. Soc. Jpn*. **2002** , *71*, 1318.
50. Falkovsky, L.A.; Varlamov, A.A. *Eur. Phys. J*. **2007**, *B. 56*, 281.
51. Fock, V.A. Principles of Quantum Mechanics; Science, Moscow, Russia, **1976**.
52. Reich, S.; Maultzsch, J.; Thomsen, C.; Ordejón, P.; *Phys. Rev.* **2002**, *B66*, 035412.
53. Davydov A.S.; Quantum mechanics; Science, Moscow, **1973**
54. Kharche, N.; ·Boykin, T. B.; Nayak ,· S. K.; *J Comput Electron* **2013** *12*, 722 **DOI**: 10.1007/s10825-013-0524-1
55. Grushevskaya, H. V.; Krylova, N. G. ; Lipnevich, I. V.; Orekhovskaja, T. I.; Egorova, V. P. ; Shulitski, B. G.; *Int. J. Mod. Phys.* **2016** *B30*, 1642018 **DOI**: 10.1142/S0217979216420182

